eJSSNT Regular Paper

e-Journal of Surface Science and Nanotechnology **19**, 70−87 (2021)

First-principles Calculations of Optical Energy Loss Functions for 30 Compound and 5 Elemental Semiconductors

Hiroshi Shinotsuka,† Hideki Yoshikawa, Shigeo Tanuma

Research and Services Division of Materials Data and Integrated System, National Institute for Materials Science, 1-1 Namiki, Tsukuba, Ibaraki 305-0044, Japan
† *Corresponding author: SHINOTSUKA.Hiroshi@nims.go.jp*

Received: 25 December, 2020; Accepted: 20 June, 2021; Published: 15 July, 2021

The energy loss function (ELF) describes the interaction between electrons and matter in solids. Electron inelastic mean free paths (IMFPs), which are important and basic parameters for describing electron inelastic scattering in matter, have been calculated theoretically from the ELFs of materials. These are essential for understanding quantitative surface spectroscopies, such as Auger electron and X-ray photoelectron spectroscopy. However, the optical constants or the ELFs of most compounds are unknown in the 10−50 eV energy range, where electron-solid interactions are strong, owing to experimental difficulty. In this study, the ELFs and the optical constants were calculated for 35 inorganic semiconductors [AgBr, AgCl, AgI, AlAs, AlN, AlSb, cubic-BN (c-BN), hexagonal-BN (h-BN), CdS, c-CdSe, h-CdSe, CdTe, C (diamond), GaAs, GaN, GaP, GaSb, GaSe, Ge, InAs, InP, InSb, PbS, PbSe, PbTe, Se, Si, c-SiC, h-SiC, SnTe, Te, c-ZnS, h-ZnS, ZnSe, and ZnTe] in a wide energy range (from 0.1 eV to 1 MeV) using first-principles calculations with FEFF and WIEN2k. The resulting 35 ELFs were evaluated using two sum rules, the *f*-sum rule and the Kramers-Kronig sum rule, resulting in average relative errors of 1.6% and 0.05%, respectively. The calculated ELFs for InAs, GaAs and InSb agreed well with the experimental ELFs obtained from the transmission electron energy loss spectroscopy (EELS) experiments and the reflection EELS experiments. The resulting database of the ELFs and the optical constants for 35 compound semiconductors was concluded to be accurate and useful for understanding the inelastic scattering processes of semiconductors with respect to IMFPs and electron stopping powers. All detailed data are available in the materials data repository provided by the National Institute for Materials Science (https://doi.org/10.34968/nims.1434).

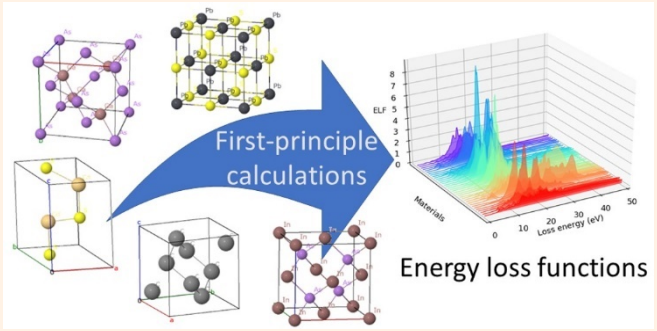

Keywords *Energy loss function; Optical constant; First-principles calculation; Compound semiconductor, Inelastic mean free paths*

I. INTRODUCTION

The energy loss function (ELF) is a fundamental physical quantity describing the interaction between electrons and matter in solids and is essential for quantitative evaluation of inelastic scattering during electron transport in solids [1]. The electron inelastic mean free paths (IMFPs) and electron stopping powers (SPs), which are important fundamental parameters in actual surface analysis by X-ray photoelectron spectroscopy (XPS), Auger electron spectroscopy (AES), and electron energy loss spectroscopy (EELS), have been calculated theoretically from the ELFs of materials [2]. In particular, the IMFP is a fundamental physical quantity used for surface quantification, representing the surface sensitivity and matrix effect of an element. Therefore, many studies have been conducted to determine the IMFPs for various materials, including elemental solids, and inorganic and organic compounds [2−11]. However, the number of the IMFPs determined remains insufficient, both in terms of the number of target materials and the applicable energy range.

In particular, the number of the ELFs of compounds remains limited, which is a bottleneck for the precise quantitative evaluation of their surfaces. Therefore, ELF measurements have been conducted for various materials and substances, but most are limited in their energy range and have accuracy problems.

Usually, the ELF can be obtained from optical constants, namely, the refractive index (n) and extinction coefficient (k). These optical constants have been measured for various materials and are summarized by Palik in a three-volume handbook, which is widely used in various studies [12–14]. However, optical constant data in the energy range of 10–50 eV, which is most important for IMFP and SP calculations, are lacking for many materials owing to the difficulty of the measurement, such as the requirement of synchrotron radiation. In particular, the measurement data are not available for most compound materials for optical constants or ELFs in this energy range, with some exceptions including GaAs and InP. In contrast, although transmission electron microscopy and reflection EELS have been used to measure optical constants or ELFs, fewer materials have been measured owing to the difficulty of sample preparation and analysis.

Therefore, we obtained a database of ELFs or optical constants for various compound semiconductors in the wide energy range from 1 eV to 1 MeV using first-principles calculations. The resulting database for the ELFs would aid the calculation of IMFPs, SPs, effective attenuation lengths (EALs), mean escape depths (MEDs), and other important physical quantities for the evaluation and the measurement of these materials by XPS, EELS, AES, and transmission electron microscopy (TEM).

The ELF is a function of energy loss (ω) and momentum transfer (q) and is given as the imaginary part of the reciprocal of the complex dielectric function, $\varepsilon(\omega, q)$. Using the ELF and Born approximation, the differential inelastic scattering cross section, per atom or molecule, for energy loss ω and momentum transfer q in an infinite medium is given by Eq. (1) [15, 16]:

$$\frac{\mathrm{d}^2\sigma}{\mathrm{d}\omega \mathrm{d}q} = \frac{1}{\pi NE}\mathrm{Im}\left[-\frac{1}{\varepsilon(\omega, q)}\right]\frac{1}{q}, \quad (1)$$

where E is the electron energy and $\mathrm{Im}[-1/\varepsilon(\omega, q)]$ is the ELF, which is now defined by the complex dielectric function, $\varepsilon(\omega, q)$. Hartree atomic units were used in Eq. (1), in which $m_e = e^2 = \hbar = 1$, where m_e is the electron rest mass, e is the elementary charge, and $\hbar$ is the reduced Planck constant.

In the limit of zero momentum transfer, the probability of inelastic scattering is proportional to the ELF, $\mathrm{Im}(-1/\varepsilon) = \varepsilon_2/(\varepsilon_1^2 + \varepsilon_2^2)$, where ε_1 and ε_2 are the real and imaginary parts of the complex dielectric constant ε. ε_1 and ε_2 are simply related to the conventional optical constants, the refractive index (n), and the extinction coefficient (k) by $\varepsilon_1 = n^2 - k^2$ and $\varepsilon_2 = 2nk$ [12].

Therefore, energy loss functions are needed for various materials in a wide energy range (typically from 1 eV to 200 keV), but optical data are lacking for most materials in the 10–50 eV energy range, where electron-solid interactions are strong, because of experimental difficulties, as stated above [11, 17, 18]. Accordingly, optical data were calculated in a wide energy range (1 eV to 1 MeV) using first-principles calculations with FEFF 8.2 [19] and WIEN2k [20], and a database of optical energy loss functions and optical constants were obtained. The target materials selected were mainly compound semiconductors for which little optical data were available. A database of the energy loss functions was then prepared for the following 35 materials between 1 eV and 1 MeV: AgBr, AgCl, AgI, AlAs, AlN, AlSb, c-BN, h-BN, CdS, CdSe, CdSe, CdTe, C (diamond), GaAs, GaN, GaP, GaSb, GaSe, Ge, InAs, InP, InSb, PbS, PbSe, PbTe, Se, Si, c-SiC, h-SiC, SnTe, Te, c-ZnS, h-ZnS, ZnSe, and ZnTe.

II. CALCULATION

This section describes the method used to calculate optical constants from first principles in a wide energy region. The imaginary part (ε_2) of dielectric function $\varepsilon = \varepsilon_1 + i\varepsilon_2$ was calculated from the WIEN2k and FEFF codes. Combining ε_2 values obtained from each approach, ε_2 was obtained over a wide loss energy range (from 0.1 eV to 1 MeV). The real part of the dielectric function (ε_1) was then calculated using the Kramers-Kronig relation. Using ε_1 and ε_2, the refractive index (n), the extinction coefficient (k), and the ELF ($\mathrm{Im}[-1/\varepsilon(\omega)]$) were finally obtained.

A. Dielectric functions from first-principles calculations

1. WIEN2k

WIEN2k calculates the electronic structure of solids based on the all-electron approach of DFT, named the full-potential linearized augmented plane wave (FLAPW) method. WIEN2k version 08.02 was used in this study. The generalized gradient approximation (GGA), as parameterized by Perdew, Burke, and Ernzerhof, was adopted for the exchange-correlation potential [21]. The spin polarization was not calculated because our target materials were not magnetic. For hexagonal crystals, optical constants under an electric field perpendicular to the c-axis of the crystal were calculated. The imaginary part of the dielectric function, ε_2, was calculated from optically allowed transition amplitudes of photon energies between 0.1 and 136 eV. Owing to computational limitations, the available loss energy is known to be less than 100 eV [20, 22].

2. FEFF

FEFF 8.2 is an automated program for calculating X-ray absorption spectra using an *ab initio* all-electron, real-space relativistic Green function [19]. This code gives photoabsorption cross-sections from any absorption edge for all elements in a compound. Only information on the crystal structure is needed to obtain the absorption spectra. This

allows ε_2 to be easily calculated, as shown below. These calculations were applied to photon energies between 10 eV and 1 MeV.

FEFF allows us to compute absorption spectra with three cards for each absorption edge (K, L_1, L_2, L_3, M_1, M_2, ⋯) of an atom. We used the XANES card near the absorption edge, the EXAFS card for tens to hundreds of eV from the absorption edge, and the FPRIME card beyond that. In all cases, the RGRID card was set to 0.01 to improve the calculation accuracy at high photon energies. Although the FPRIME card gives the imaginary part of the atomic scattering factor, $f_2(\omega)$, the XANES and EXAFS cards give the optical absorption spectra $\mu(\omega)$, which can be converted to $f_2(\omega)$ using Eq. (2):

$$f_2(\omega) = \frac{\omega}{4\pi\alpha}\mu(\omega) \ \text{(in a. u.)}, \tag{2}$$

where α = 1/137.0359895 is the fine-structure constant. We connected $f_2(\omega)$ values obtained from the XANES, EXAFS, and FPRIME cards, and constructed $f_2(\omega)$ in a wide photon energy range from a single absorption edge. For the outer-shell orbital contribution to valence electrons, we confirmed that it was better to use FPRIME cards only. In the same manner, $f_2(\omega)$ was obtained from all the absorption edges of the same atom. By combining them, $f_2(\omega)$ was obtained for one atom. As each absorption edge has a different energy grid of absorption spectral data, the data needed to be interpolated when added together.

Next, the imaginary part of the atomic scattering factor $f_2(\omega)$ per molecule was calculated for a compound with a composition represented by $A_{m_A}B_{m_B}$. In this case, by labeling the imaginary part of the atomic scattering factor of an atom X, as $f_{2,X}(\omega)$, the scattering factor $f_2(\omega)$ per molecule can be simply calculated using Eq. (3):

$$f_2(\omega) = \sum_X m_X f_{2,X}(\omega) \ \ (X = A, B) \tag{3}$$

The imaginary part of the dielectric function $\varepsilon_2(\omega)$ is calculated using $f_2(\omega)$ [23]:

$$\varepsilon_2(\omega) = \frac{2c_6}{\omega^2} f_2(\omega), \tag{4}$$

$$c_6 = 415.1792338\frac{\rho}{F_W}, \tag{5}$$

where ω is the photon energy (eV), ρ is the mass density of a material (g cm^{-3}), and F_W is the molecular weight of the compound (g mol^{-1}).

A dielectric function has not previously been created by connecting the results of WIEN2k and FEFF calculations. Although Rehr and coworkers [24–26] have calculated the dielectric function in the wide loss energy range using only FEFF, the accuracy of the calculation below 50 eV was questionable, especially around the prominent energy loss region.

B. Determination of energy loss function

We calculated ε_2 using two methods, WIEN2k for 0.1–136 eV and FEFF from 10 eV to 1 MeV. For example, Figure 1 shows ε_2 as a function of energy loss ω for InAs and PbS below 100 eV, with ε_2 from WIEN2k and FEFF overlapping well at 30 and 50 eV, respectively. Similarly, for all 35 materials, the ε_2 values overlapped well at a certain loss energy between 30 and 80 eV, allowing them to connect at the loss energy. Table 1 shows the connection energies of the 35 materials in this study. Finally, a dataset of ε_2 calculated by WIEN2k and FEFF for each compound was prepared for photon energies from 0.1 eV to 1 MeV.

The real part of the dielectric function ε_1 was calculated from ε_2 using the Kramers-Kronig relation [27]:

$$\varepsilon_1(\omega) = 1 + \frac{2}{\pi}P\int_0^\infty \frac{\omega'\varepsilon_2(\omega')}{(\omega')^2 - \omega^2}d\omega', \tag{6}$$

where P is the Cauchy principal value. The actual integration range of Eq. (6) was from 0.1 eV to 1 MeV. The algorithm used to numerically calculate the Kramers-Kronig relation is described in Appendix.

The optical ELF was then calculated from the data sets of

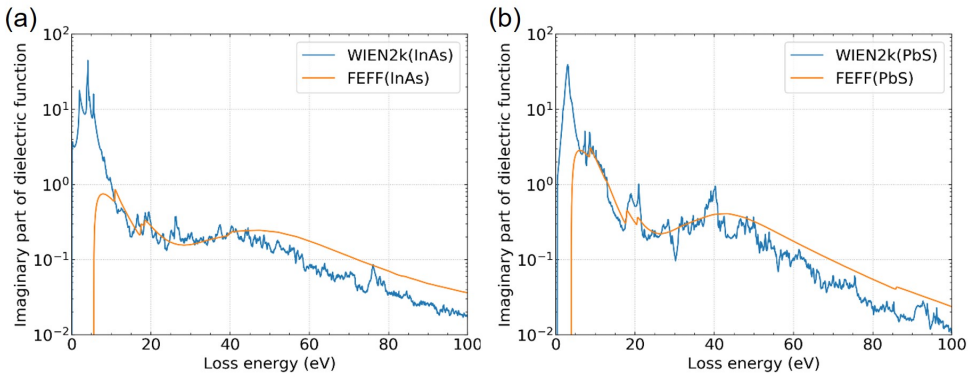

Figure 1: Plots of the imaginary part of the dielectric function (ε_2) as functions of energy loss for (a) InAs and (b) PbS. Blue and orange solid lines represent ε_2 calculated by WIEN2k and FEFF, respectively.

Table 1: Connection energies for the 35 materials in this study. ε_2 from WIEN2k is used below the given energy, while ε_2 from FEFF is used above.

Material	Connection energy (eV)
AgBr	30
AgCl	30
AgI	30
AlAs	50
AlN	70
AlSb	50
c-BN	80
h-BN	80
CdS	30
c-CdSe	30
h-CdSe	30
CdTe	30
C (diamond)	50
GaAs	50
GaN	50
GaP	50
GaSb	50
GaSe	46
Ge	50
InAs	30
InP	30
InSb	30
PbS	50
PbSe	50
PbTe	50
Se	45
Si	50
c-SiC	50
h-SiC	50
SnTe	37
Te	37
c-ZnS	50
h-ZnS	50
ZnSe	50
ZnTe	38

ε_1 and ε_2 with the following Eq. (7):

$$\mathrm{Im}\left[-\frac{1}{\varepsilon(\omega)}\right] = \frac{\varepsilon_2(\omega)}{\varepsilon_1(\omega)^2 + \varepsilon_2(\omega)^2}, \tag{7}$$

From the complex dielectric function $\varepsilon_1 + i\varepsilon_2$, the complex refractive index, $n + ik$, where n is the refractive index and k is the extinction coefficient, can be obtained easily. Notably, erroneous conversion often occurs between the complex dielectric function and complex refractive index (Henke [23] reports inaccurate expressions). Using the relation between the complex dielectric function and complex refractive index, $\varepsilon_1 + i\varepsilon_2 = (n + ik)^2$, mutual conversion was performed as follows:

$$\varepsilon_1 = n^2 - k^2, \tag{8}$$

Table 2: Crystal information used in the FEFF and WIEN2k calculations for each material in this study. Cell parameters are obtained from the AtomWork database [28]. Crystal information for all but eight materials [c-CdSe, C (diamond), Ge, Se, Si, h-SiC, Te, and h-ZnS] is taken from Ref. 6.

Material	Space group	Cell parameter
AgBr	$Fm\bar{3}m$	a = 0.5775 nm
AgCl	$Fm\bar{3}m$	a = 0.5543 nm
AgI	$P6_3mc$	a = 0.45856 nm
		c = 0.749 nm
		γ = 120°
AlAs	$F\bar{4}3m$	a = 0.56605 nm
AlN	$P6_3mc$	a = 0.311 nm
		c = 0.498 nm
		γ = 120°
AlSb	$F\bar{4}3m$	a = 0.6135 nm
c-BN	$F\bar{4}3m$	a = 0.36159 nm
h-BN	$P6_3/mmc$	a = 0.25045 nm
		c = 0.6606 nm
		γ = 120°
CdS	$P6_3mc$	a = 0.4142 nm
		c = 0.6724 nm
		γ = 120°
c-CdSe	$F\bar{4}3m$	a = 0.604 nm
h-CdSe	$P6_3mc$	a = 0.4299 nm
		c = 0.701 nm
		γ = 120°
CdTe	$F\bar{4}3m$	a = 0.6482 nm
C (diamond)	$Fd\bar{3}m$	a = 0.35669 nm
GaAs	$F\bar{4}3m$	a = 0.56532 nm
GaN	$P6_3mc$	a = 0.31891 nm
		c = 0.51855 nm
		γ = 120°
GaP	$F\bar{4}3m$	a = 0.54508 nm
GaSb	$F\bar{4}3m$	a = 0.60959 nm
GaSe	$P6_3/mmc$	a = 0.375 nm
		c = 1.5995 nm
		γ = 120°
Ge	$Fd\bar{3}m$	a = 0.56575 nm
InAs	$F\bar{4}3m$	a = 0.60577 nm
InP	$F\bar{4}3m$	a = 0.58687 nm
InSb	$F\bar{4}3m$	a = 0.64794 nm
PbS	$Fm\bar{3}m$	a = 0.59315 nm
PbSe	$Fm\bar{3}m$	a = 0.61213 nm
PbTe	$Fm\bar{3}m$	a = 0.64541 nm
Se	$P3_221$	a = 0.43552 nm
		c = 0.49495 nm
		γ = 120°
Si	$Fd\bar{3}m$	a = 0.54309 nm
c-SiC	$F\bar{4}3m$	a = 0.43581 nm
h-SiC	$P6_3mc$	a = 0.3076 nm
		c = 0.5048 nm
		γ = 120°
SnTe	$Fm\bar{3}m$	a = 0.6323 nm
Te	$P3_221$	a = 0.44469 nm
		c = 0.59149 nm
		γ = 120°
c-ZnS	$F\bar{4}3m$	a = 0.54102 nm
h-ZnS	$P6_3mc$	a = 0.3822 nm
		c = 0.626 nm
		γ = 120°
ZnSe	$F\bar{4}3m$	a = 0.56692 nm
ZnTe	$F\bar{4}3m$	a = 0.61026 nm

$$\varepsilon_2 = 2nk\,, \tag{9}$$

$$n = \sqrt{\frac{|\varepsilon| + \varepsilon_1}{2}}, \tag{10}$$

$$k = \sqrt{\frac{|\varepsilon| - \varepsilon_1}{2}}, \tag{11}$$

where $|\varepsilon| = \sqrt{\varepsilon_1^2 + \varepsilon_2^2}$.

Only structural information of the crystal lattice was needed for first-principles calculation of the dielectric function. Table 2 shows crystal information for the inorganic compounds used in the WIEN2k [20] and FEFF [19] calculations [28]. Crystal information for all but eight materials [c-CdSe, C (diamond), Ge, Se, Si, h-SiC, Te, and h-ZnS] are taken from Ref. 11.

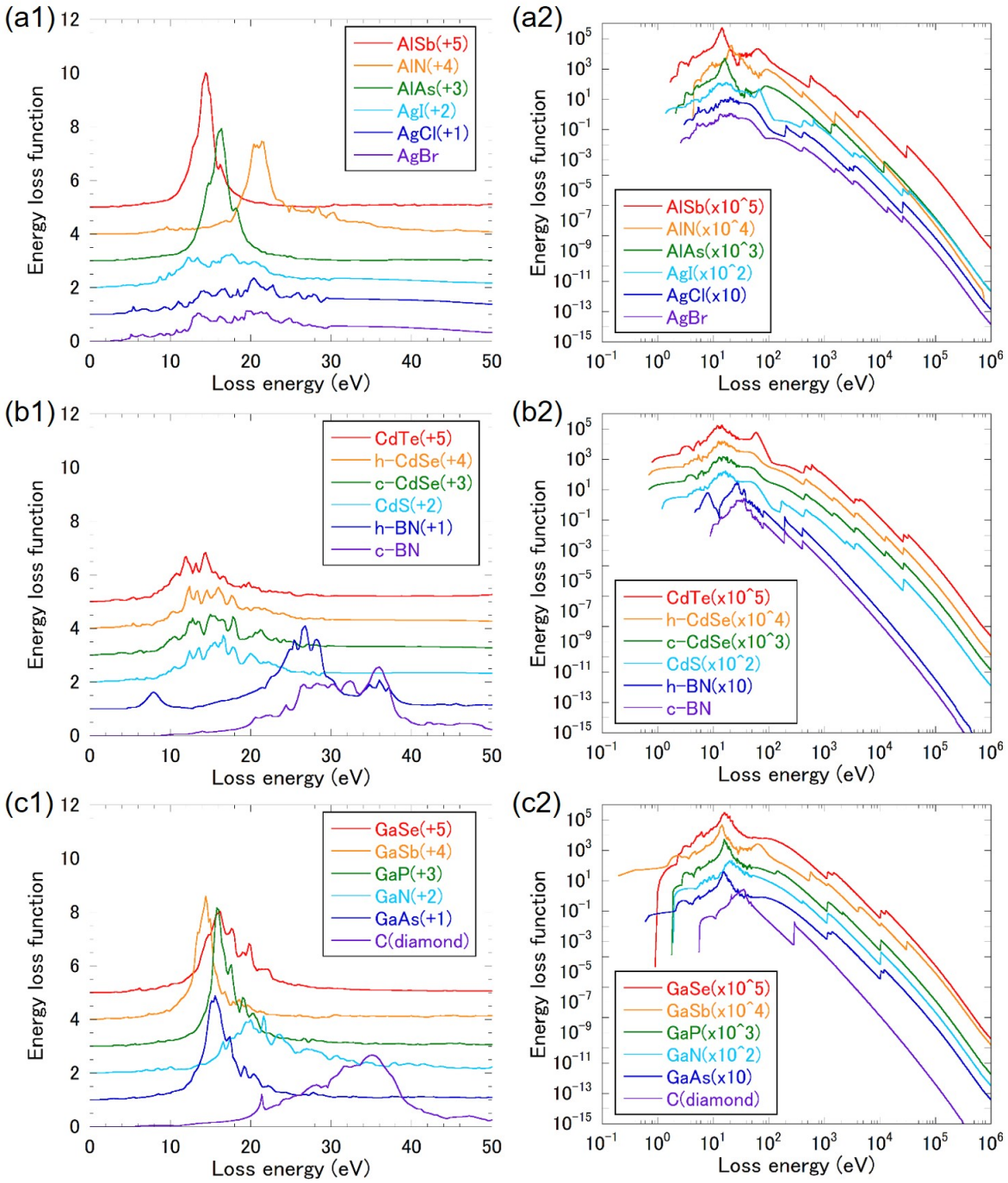

Figure 2: Energy loss functions for the 35 materials in this study. Lefthand figures are bilinear plots, and righthand figures are log-log plots. The vertical axis is shifted for each material to avoid overlapping of each graph.

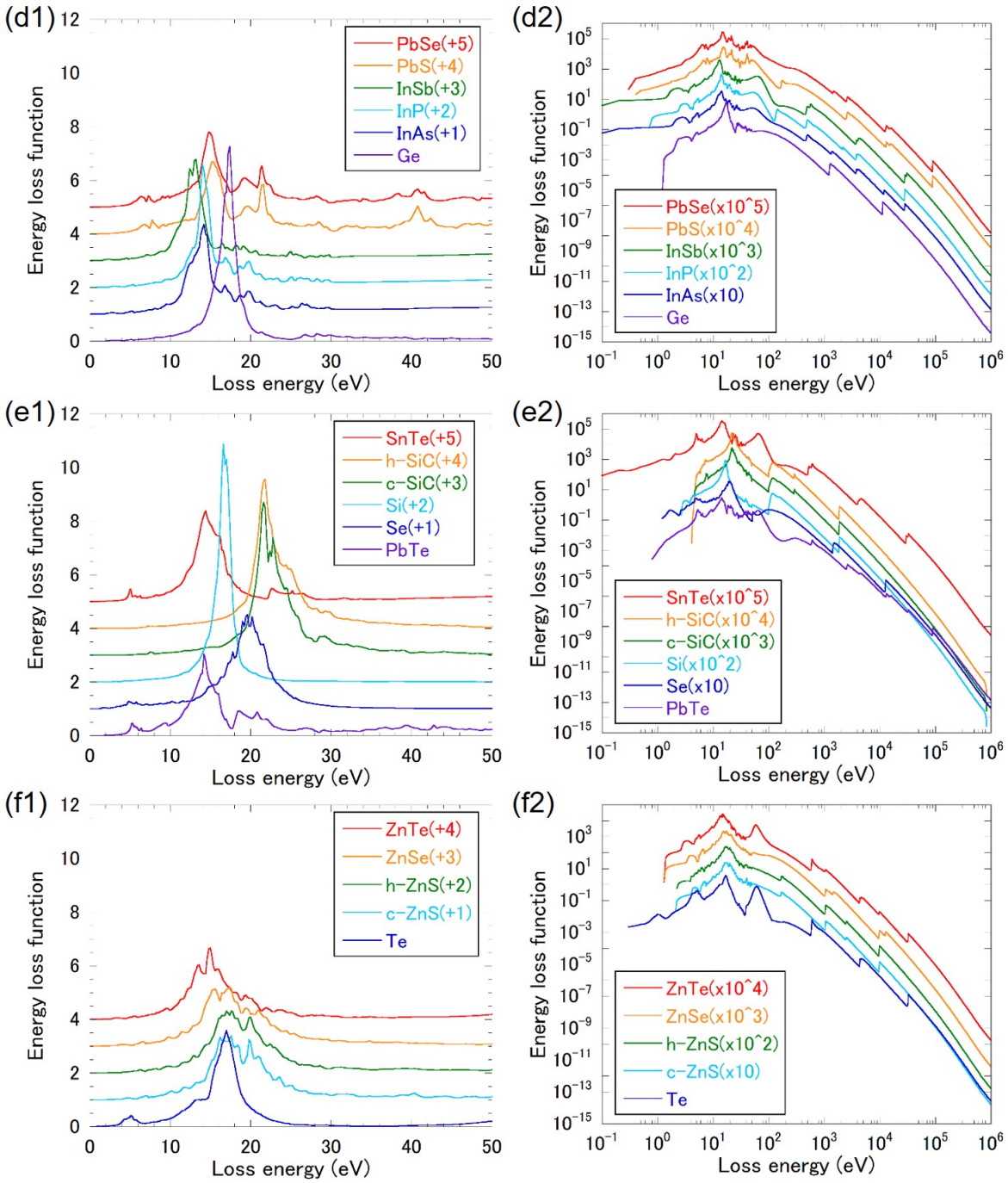

Figure 2: (Continued)

III. RESULTS

The results calculated using WIEN2k and FEFF for the 35 semiconductors are shown in Figures 2–6: Figure 2 shows ELFs, Figure 3 shows the refractive index (n), Figure 4 shows the extinction coefficients (k), Figure 5 shows the real part of the dielectric function (ε_1), and Figure 6 shows the imaginary part of the dielectric function (ε_2). All numerical data can be obtained from the materials data repository provided by the National Institute for Materials Science [29]. Herein, the ELF results, which are strongly related to surface analysis, are described.

A. ELFs

Figure 2 shows plots of the ELFs for the 35 materials. These plots were linear in the energy range of 0–50 eV and log-log for the range of 0 eV to 1 MeV. Above 100 eV, all ELFs had a similar shape, and decreased with increasing

excitation energy. Absorption edges related to the excitation of inner-shell electrons were observed, from which the constituent elements of a material can be identified. The physical properties of a material mainly originate from the difference in shape and intensity of the ELF below 100 eV. A prominent sharp peak in the ELF, related to a pseudo-plasmon excitation, was observed for GaAs, GaSb, InAs, Si, and other materials. In these cases, the pseudo-plasmon energies [$E_p = 28.8(N_v\rho/M)^{1/2}$, where N_v is the number of valence electrons per molecule, ρ is the bulk density (g cm^{-3}), and M is the molecular weight] agreed with the peak position of the ELF data. However, materials with broad ELF shapes, such as AgBr and AgCl, were dominated by single-electron excitations rather than pseudo-plasmon excitations.

Some materials were missing ELF and ε_2 data at very high loss energy due to data processing in FEFF, including AlN, c-BN, h-BN, C (diamond), Si, c-SiC, and h-SiC. The ELFs in this range were sufficiently small, so that the influence on the results is negligible.

B. Evaluations of ELFs

The internal consistency of our ELF data was checked for each compound using the oscillator-strength or the f-sum rule and a limiting form of the Kramers-Kronig integral (or

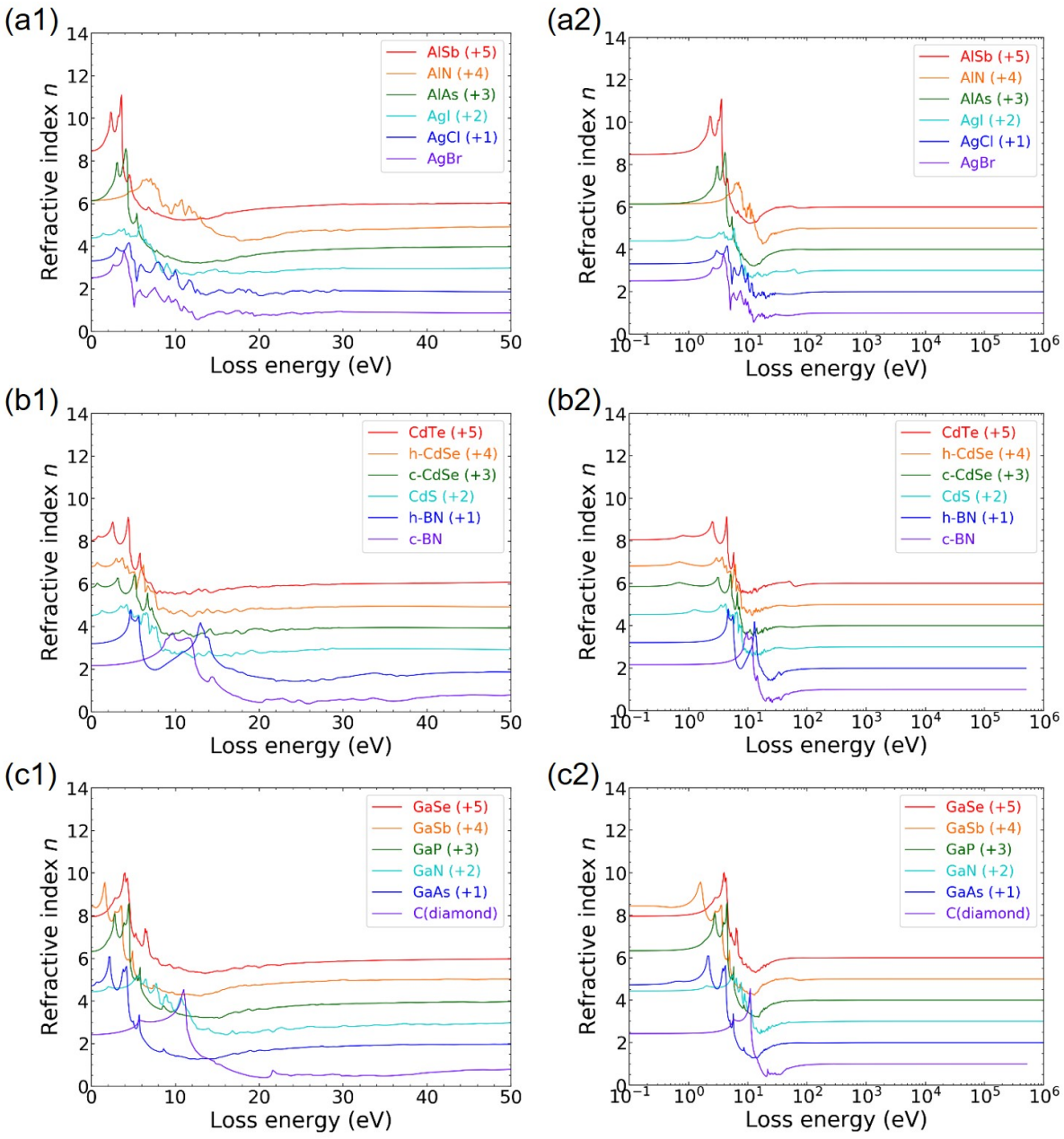

Figure 3: Refractive indexes for the 35 materials in this study. Lefthand figures are bilinear plots, and righthand figures are log-linear plots. The vertical axis is shifted for each material to avoid overlapping of each graph.

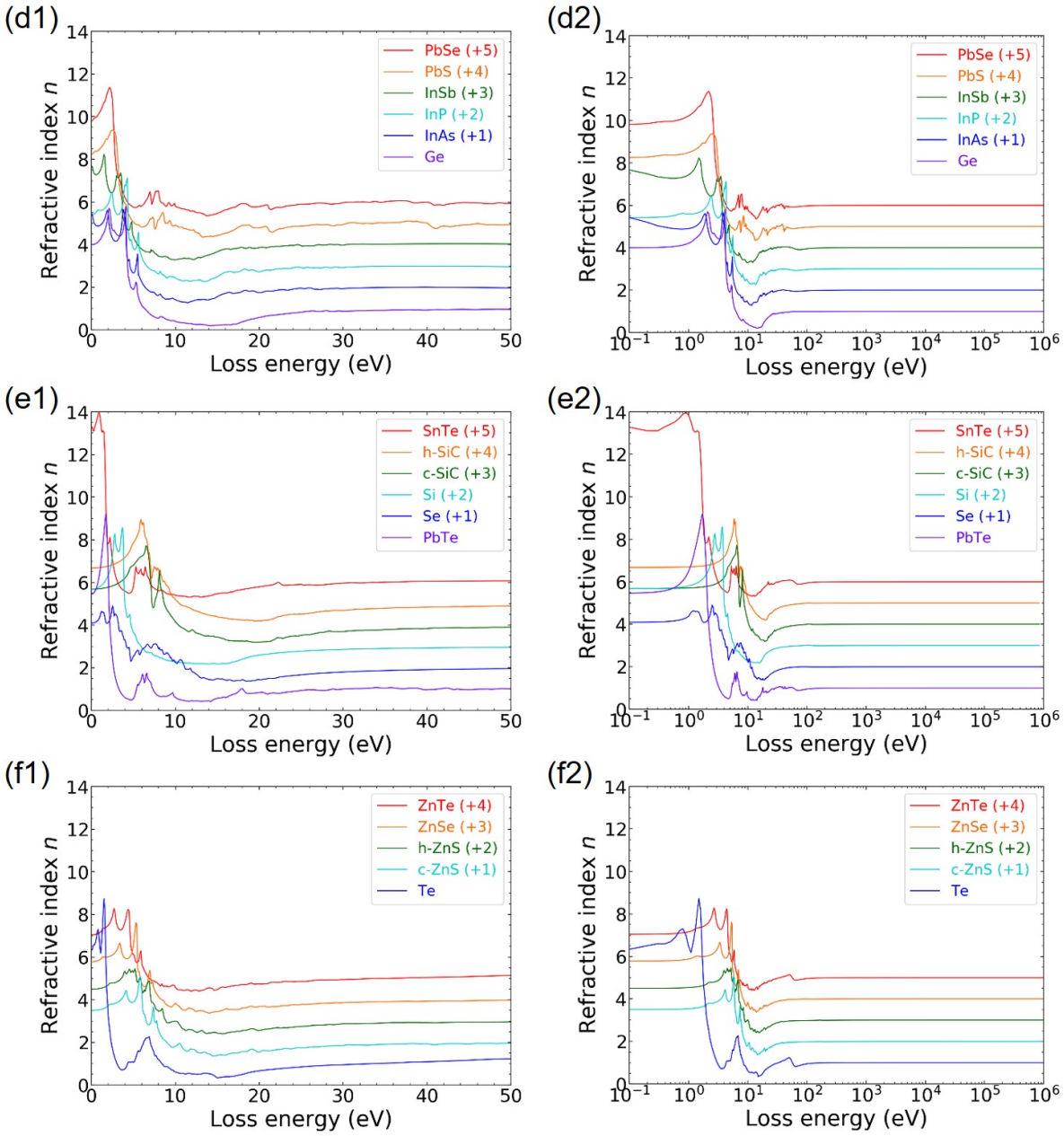

Figure 3: (Continued)

the KK-sum rule) [5, 30]. The *f*-sum can be evaluated as the total effective number of electrons per molecule, Z_{eff}, contributing to inelastic scattering using Eq. (12):

$$Z_{\text{eff}} = \left(\frac{2}{\pi\hbar^2\Omega_{\text{p}}^2}\right)\int_{\Delta E_{\text{min}}}^{\Delta E_{\text{max}}} (\Delta E)\text{Im}\left[-\frac{1}{\varepsilon(\Delta E)}\right]\text{d}(\Delta E), \quad (12)$$

where $\Delta E = \hbar\omega$, $\Omega_{\text{p}} = (4\pi n_{\text{a}} e^2/m)^{1/2}$, $n_{\text{a}} = N_{\text{a}}\rho/M$ is the density of atoms, N_{a} is the Avogadro number, ρ is the mass density, and M is the molecular weight. The minimum and maximum energy losses in Eq. (12), ΔE_{min} and ΔE_{max}, were 0.1 eV and 1 MeV, respectively. The *f*-sum for ε_2 is similar, as shown in Eq. (13):

$$Z_{\text{eff},\varepsilon_2} = \left(\frac{2}{\pi\hbar^2\Omega_{\text{p}}^2}\right)\int_{\Delta E_{\text{min}}}^{\Delta E_{\text{max}}} (\Delta E)\varepsilon_2(\Delta E)\text{d}(\Delta E) \quad (13)$$

In the limit $\Delta E_{\text{max}} \to \infty$, both Z_{eff} and $Z_{\text{eff},\varepsilon_2}$ are expected to approach Z, the total number of electrons per molecule. The KK-sum can be expressed as shown in Eq. (14):

$$P_{\text{eff}} = \frac{2}{\pi}\int_{\Delta E_{\text{min}}}^{\Delta E_{\text{max}}} (\Delta E)^{-1}\text{Im}\left[-\frac{1}{\varepsilon(\Delta E)}\right]\text{d}(\Delta E) + \text{Re}\left[\frac{1}{\varepsilon(\Delta E_{\text{min}})}\right], \quad (14)$$

where $\mathrm{Re}[1/\varepsilon(\Delta E_{\min})] \simeq n^{-2}(\Delta E_{\min})$ when $\Delta E_{\min}$ is sufficiently small. In the limit $\Delta E_{\max} \to \infty$, $P_{\mathrm{eff}} \to 1$ is expected.

Table 3 lists the errors in the *f*-sum and KK-sum rules for each material, which are the differences between the computed values of Z_{eff} and P_{eff}, and the expected values (total number of electrons per molecule and unity, respectively). The error in Z_{eff} ranged from −2.9% to +1.7%, and the mean absolute percentage error (MAPE) was 1.6%. The MAPE is defined as shown in Eq. (15):

$$\mathrm{MAPE}\ (\%) = \frac{100}{n}\sum_{i=1}^{n}\left|\frac{y_i^{\mathrm{Calc}} - y_i^{\mathrm{True}}}{y_i^{\mathrm{True}}}\right|, \qquad (15)$$

where y_i^{True} is a true datum and y_i^{Calc} a calculated datum for the *i*-th material. Most materials (65%) had an error of less than 2.0%. Table 3 shows that $Z_{\mathrm{eff},\varepsilon_2}$ obtained with the *f*-sum rule for ε_2 agreed well with Z_{eff} obtained with the *f*-sum rule for the ELF. The error in P_{eff} ranged from −0.43% to +0.06%, and the MAPE was 0.05% for all 35 materials. Unsurprisingly, the KK-sum was almost exactly constant because Eq. (13) is derived from the causality itself.

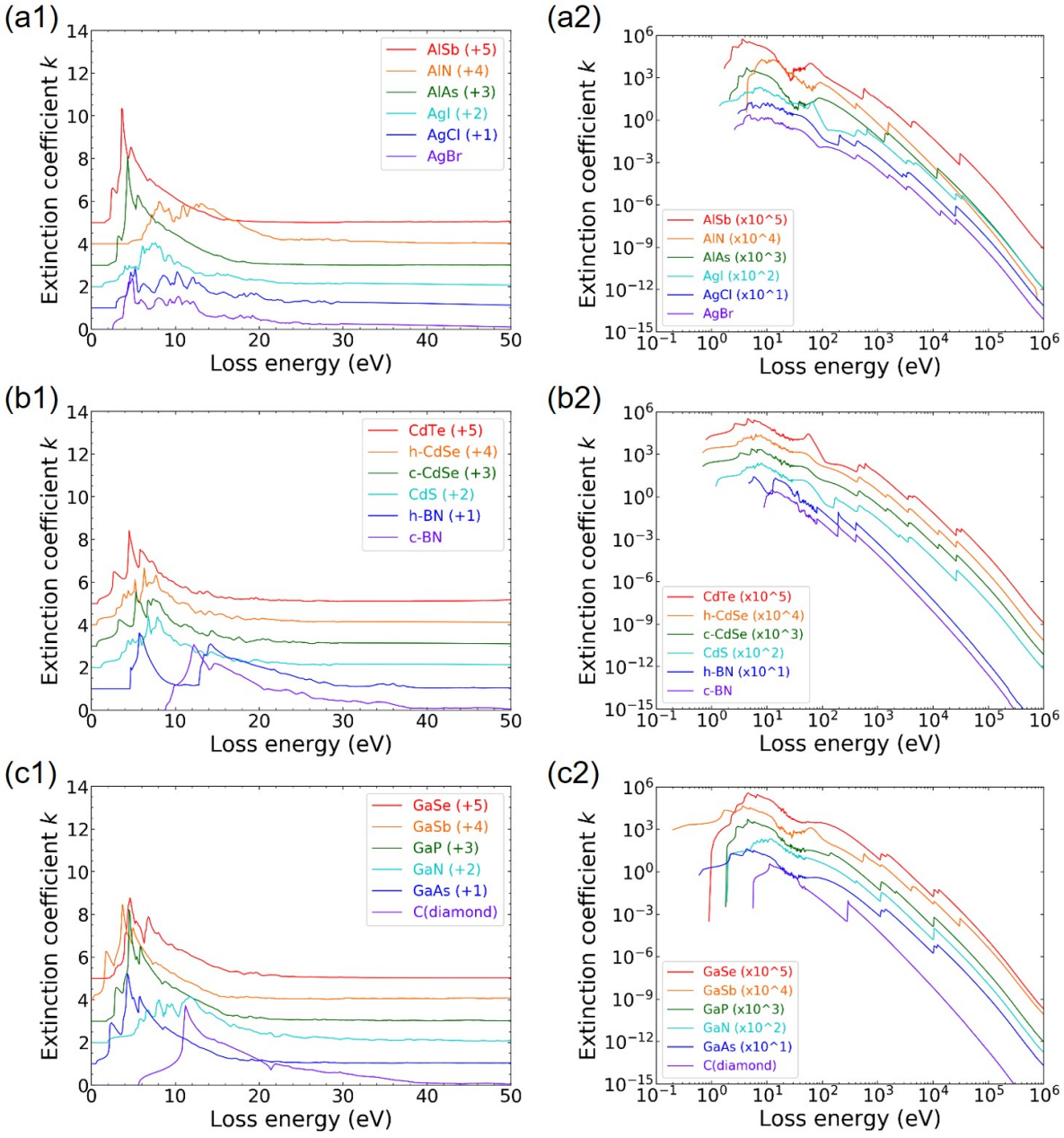

Figure 4: Extinction coefficients for the 35 materials in this study. Lefthand figures are bilinear plots, and righthand figures are log-log plots. The vertical axis was shifted for each material to avoid overlapping of each graph.

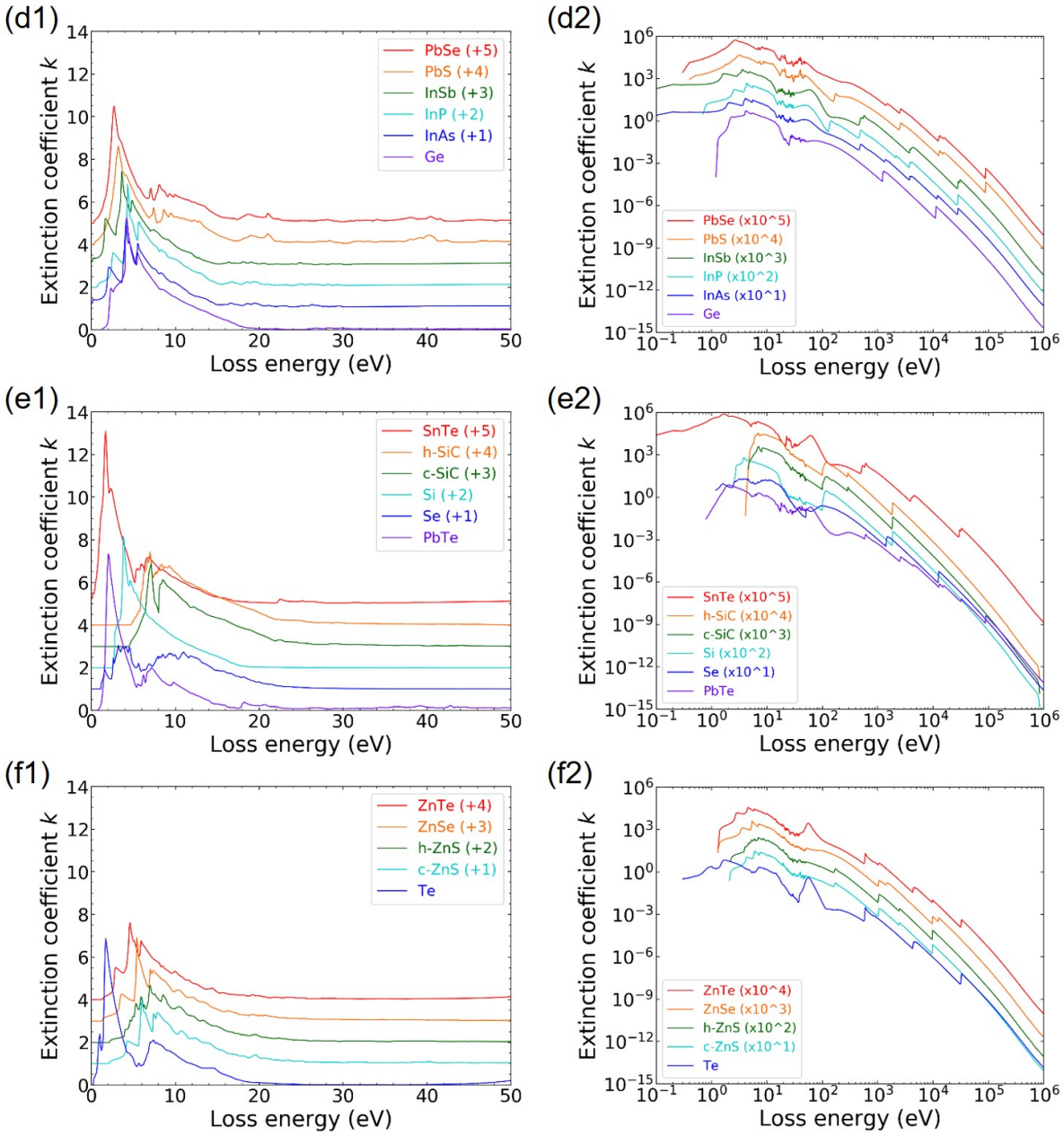

Figure 4: (Continued)

Table 3 shows that both the *f*-sum and KK-sum errors are sufficiently small, with the KK-sum error being particularly small.

IV. DISCUSSION

In this section, several our calculated results are compared with the experimental data.

A. Comparison of ELFs with experimental data

Figure 7 shows the ELFs calculated by WIEN2k and FEFF for InAs, PbS, GaAs, and InSb together with the ELFs obtained from the transmission EELS experiments by von Festenberg [31], those analyzed by Chen *et al.* [32], those obtained from the measured optical constants by Palik [12–14], and those obtained from the reflection EELS experiments by Jin *et al.* [17]. For InAs in Figure 7(a), the calculated ELF agreed with the ELF of von Festenberg. The plasmon peak position obtained from the calculated ELF was 14.2 eV, which agreed well with the value of 13.8 eV obtained from the Festenberg ELF. Furthermore, the microstructure found in the measured range of 18–22 eV agreed well with the microstructure obtained by calculation. On the other hand, we see a large difference between our ELF and the ELF calculated from optical constants by Palik. As noted by Palik [12–14], the InAs sample of Ehrenreich and Philipp

probably had a ~2-nm-thick native oxide on its surface. Therefore, it is unsurprising that the InAs ELF in Figure 7(a) from the Palik optical data differed considerably from the other ELFs. In particular, the plasmon peak from the Palik data was at 13.0 eV and was much weaker than the peaks for other ELFs in Figure 7(a).

For PbS in Figure 7(b), as a whole the calculated ELF did not coincide well with the ELF obtained from the experimental data of Palik. However, the three peaks at 15.2, 20.6, and 22.7 eV in the experimental data agreed well with the calculated peak positions of 15.4, 19.6, and 21.6 eV. The calculated ELF also had small peaks at 6.8 and 7.8 eV, which corresponded well with the measured shoulder structure at 6−10 eV. The differences between the peak heights and peak widths for two ELFs are not known exactly, but they are thought to be originated from surface oxidation and crystal imperfection, since the sample used in the experiment was a natural crystal. Furthermore, the sum rule errors for our ELF for PbS are less than 3% as shown in Table 3. Then, our calculated ELF for PbS is superior to the experimental ELF of Palik.

Figure 7(c) shows that the GaAs ELF from WIEN2k for energy losses up to 50 eV is in excellent agreement with the ELF determined by Jin *et al.* from angle resolved EELS data

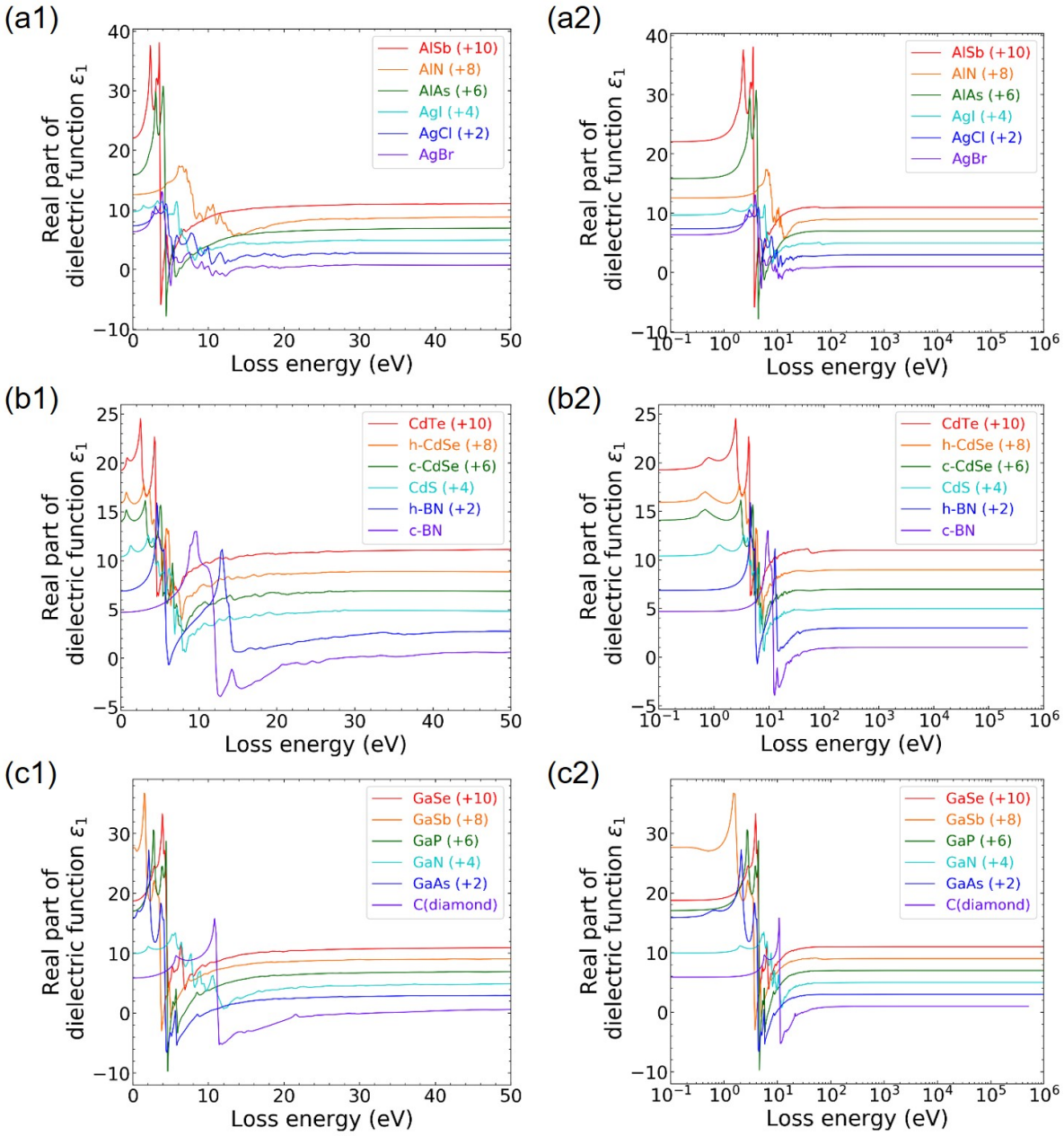

Figure 5: Real part of the dielectric functions for the 35 materials in this study. Lefthand figures are bilinear plots, and righthand figures are log-linear plots. The vertical axis is shifted for each material to avoid overlapping of each graph.

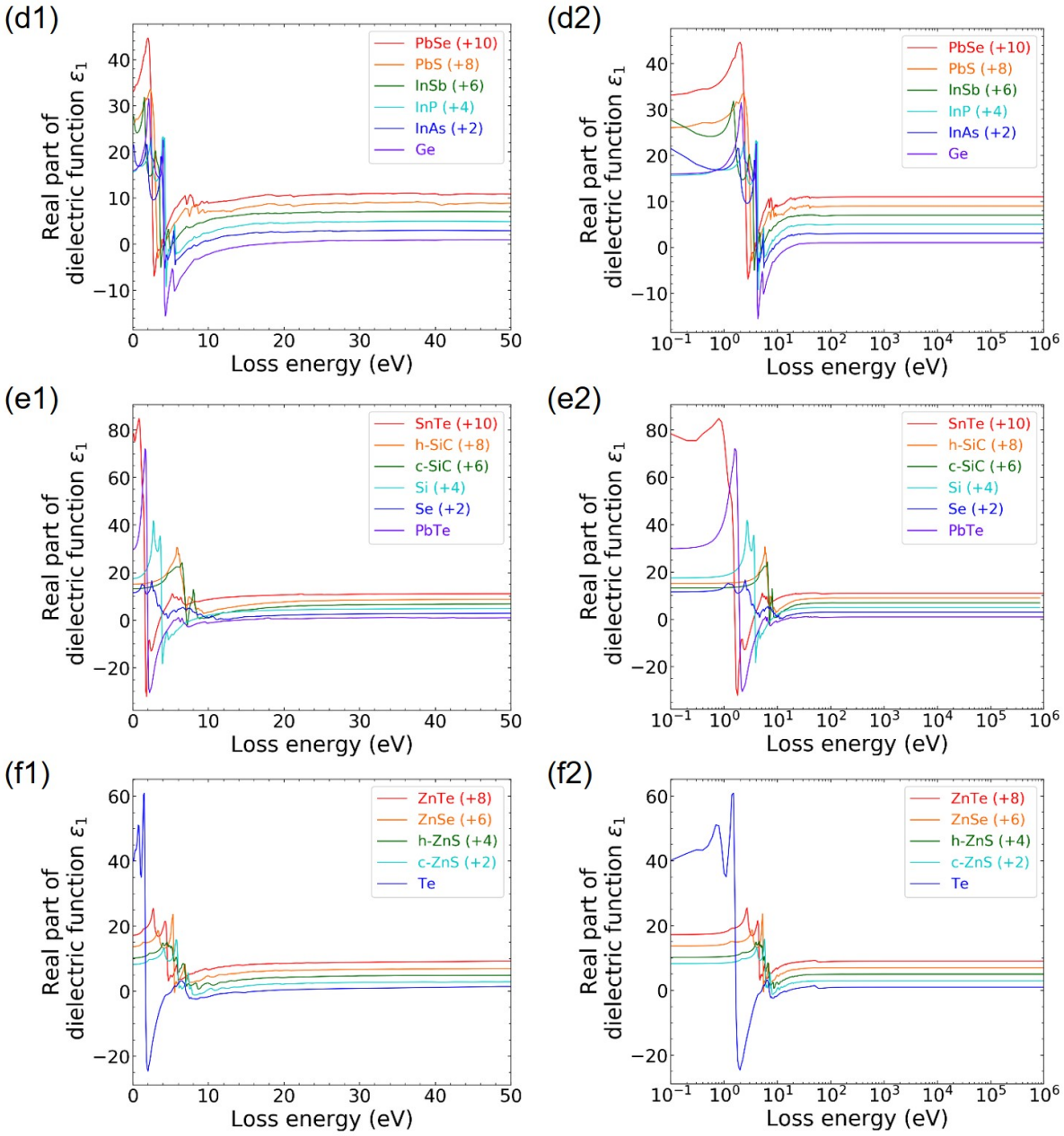

Figure 5: (Continued)

using target factor analysis method. It is also in good agreement with the ELF obtained by Chen *et al.* over 0 eV to 25 eV. On the other hand, our ELF is very different from the ELF that was calculated from experimental optical constants tabulated by Palik. The details of the comparison between our ELF and Palik ELF were figured in our previous paper [11].

The ELF for InSb from the WIEN2k is shown in Figure 7(d) and is in good agreement with the ELF determined by von Festenberg [31] from transmission-EELS experiments. The ELF from the optical data of Palik shows a plasmon peak at 12.0 eV that is much weaker than the plasmon peak found in the ELFs from WIEN2k and von Festenberg. The optical constants tabulated by Palik for InSb were obtained from the reflectivity measurements of Philipp and Ehrenreich [33] in the energy range from 6 to 24 eV. Their InSb sample was prepared and handled in the poor vacuum conditions, and it is then likely that the InSb sample had a surface oxide.

We conclude that the ELFs of InAs, PbS, GaAs, and InSb obtained from WIEN2k are superior to the ELFs obtained from published optical data [12–14]. We also point out that the resulting 35 ELFs gave excellent sum rule results, as shown in Table 3. Therefore, we could conclude that a sufficiently practical database of the ELFs for compound semiconductors has been constructed.

B. Band gap energies

When calculating IMFPs from ELFs with the full Penn algorithm using the Boutboul approach, the values of the band gap are known to significantly influence the resulting IMFP values in the low energy region [11]. In contrast, it is generally difficult to measure the band gap energies of non-conductors precisely, resulting in their values obtained from the literature varying widely [10]. Band gap energies were then determined from the ELFs calculated with WIEN2k for compounds and compared with the measured values (median values in the literature).

Figure 8 shows the resulting band gaps obtained with WIEN2k for 35 materials as a function of measured band gap energies. The solid line shows the case where the measured (E_g^{mes}) and calculated band gap values (E_g^{WIEN2k}) are equal. Major parts of band gaps calculated with WIEN2k (27 of the 35 materials) were smaller than the measured band gaps. This tendency was consistent with the fact that the band gaps obtained by DFT calculations using the local density approximation [34] or GGA [21] tend to be smaller than measured band gaps [34].

The dotted line indicates the curve fit results of band gaps obtained from WIEN2k, which represents $E_g^{WIEN2k} =$

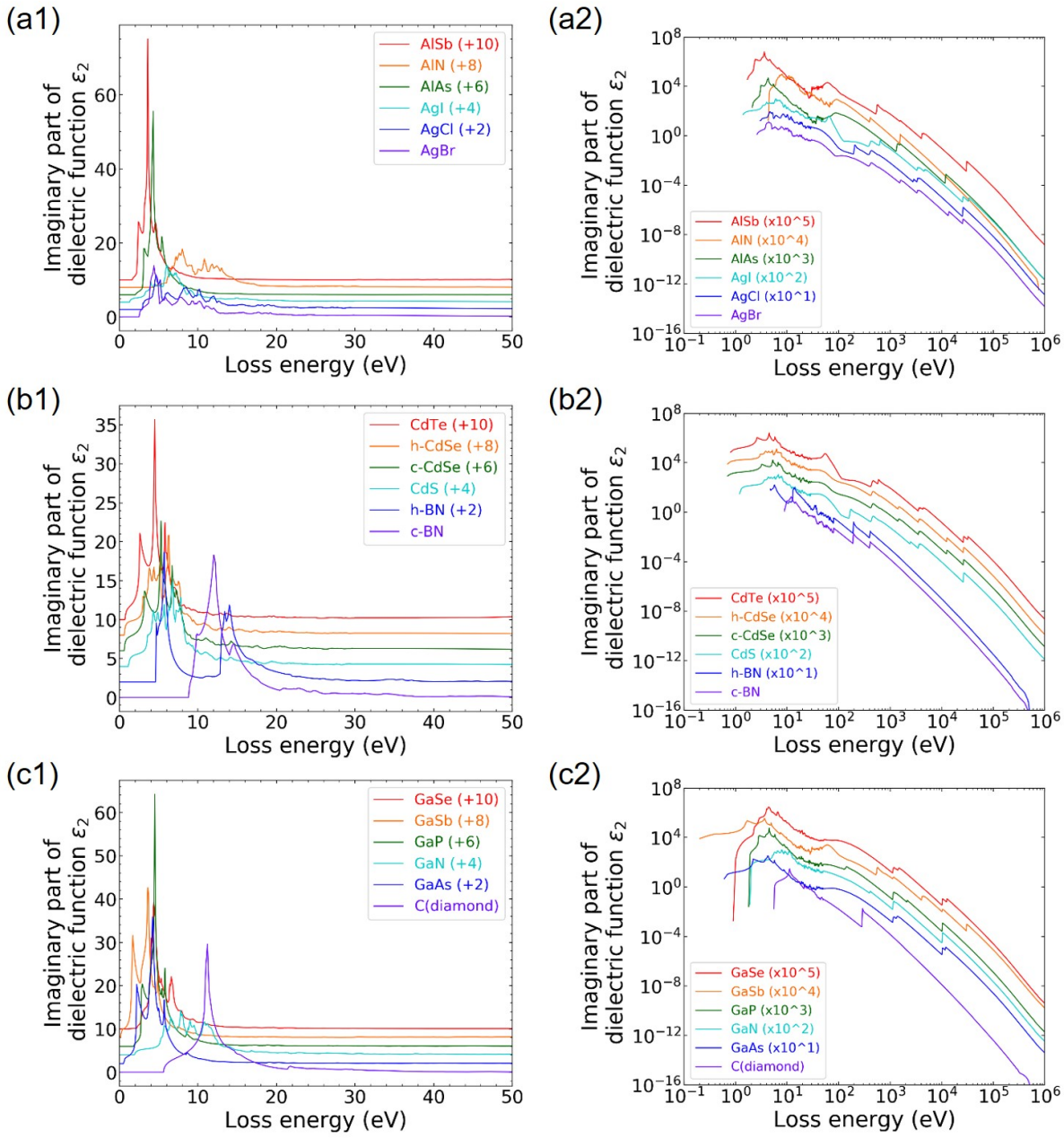

Figure 6: Energy loss functions for the 35 materials in this study. Lefthand figures are bilinear plots, and righthand figures are log-log plots. The vertical axis is shifted for each material to avoid overlapping of each graph.

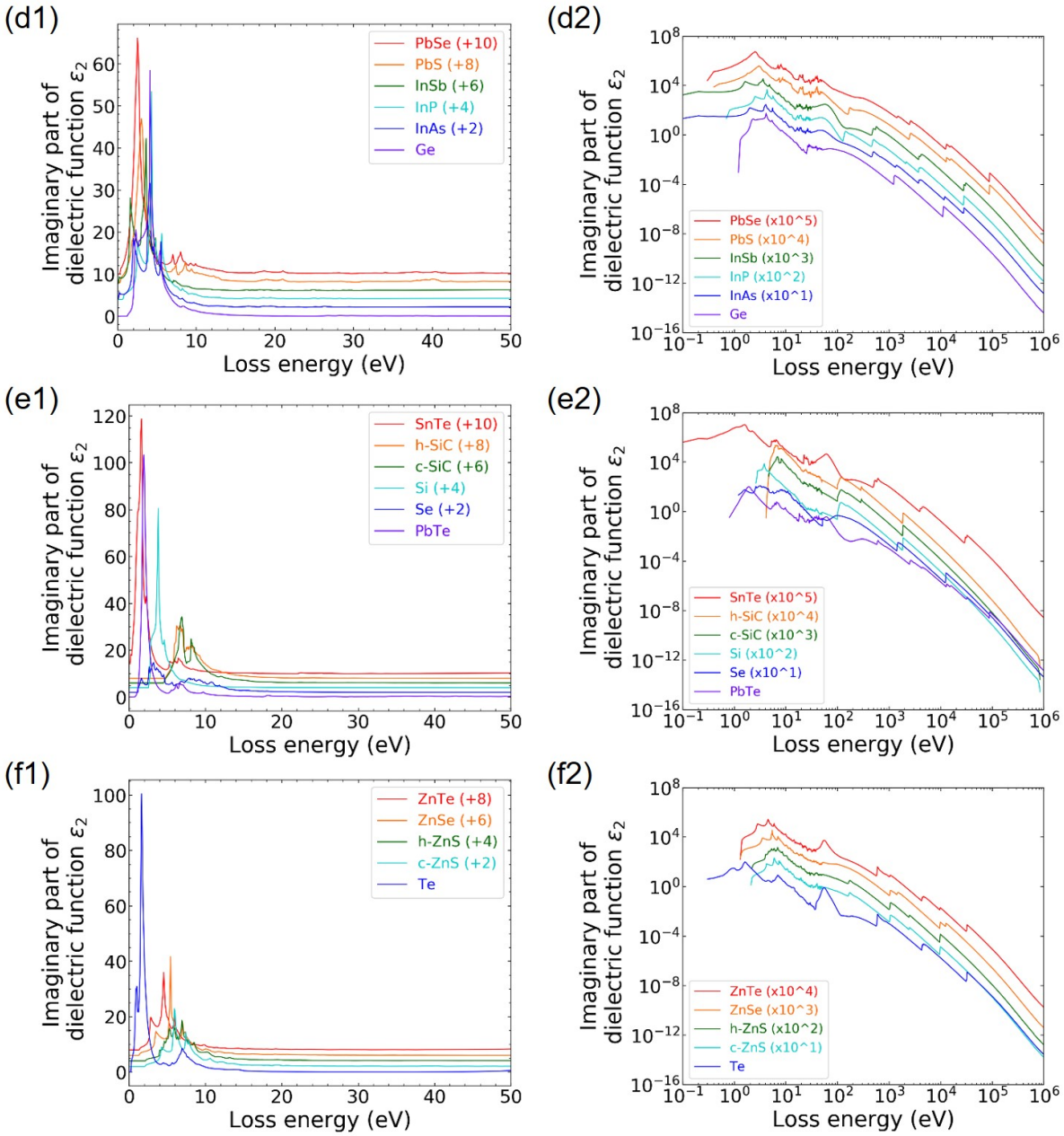

Figure 6: (Continued)

$0.88E_g^{mes}$ ($\pm 0.06E_g^{mes}$). The root-mean-square differences for measured and calculated band gaps was 1.0 eV. Therefore, the differences between the calculated and measured band gap energies were not large. This indicated that there was no problem in the calculation of IMFPs above 50 eV when using the calculated band gap energy obtained from WIEN2k [11].

V. CONCLUSION

The dielectric function and optical constants for 35 semiconductors in the photon energy range from 0.1 eV to 1 MeV were calculated using first-principles calculation programs WIEN2k and FEFF. The imaginary parts of the dielectric functions of the low-loss energy side and high-loss energy side were calculated using WIEN2k and FEFF, respectively, and were connected at a certain loss energy between 30 and 80 eV. The connection energies were determined for each material. The real part of the dielectric function was calculated from the imaginary part of the dielectric function using the Kramers-Kronig relation. The optical ELF, refractive index, and extinction coefficient were also calculated. All values determined here can be obtained from the materials data repository provided by the National Institute for Materials Science [29].

The ELFs calculated by WIEN2k and FEFF for InAs, PbS,

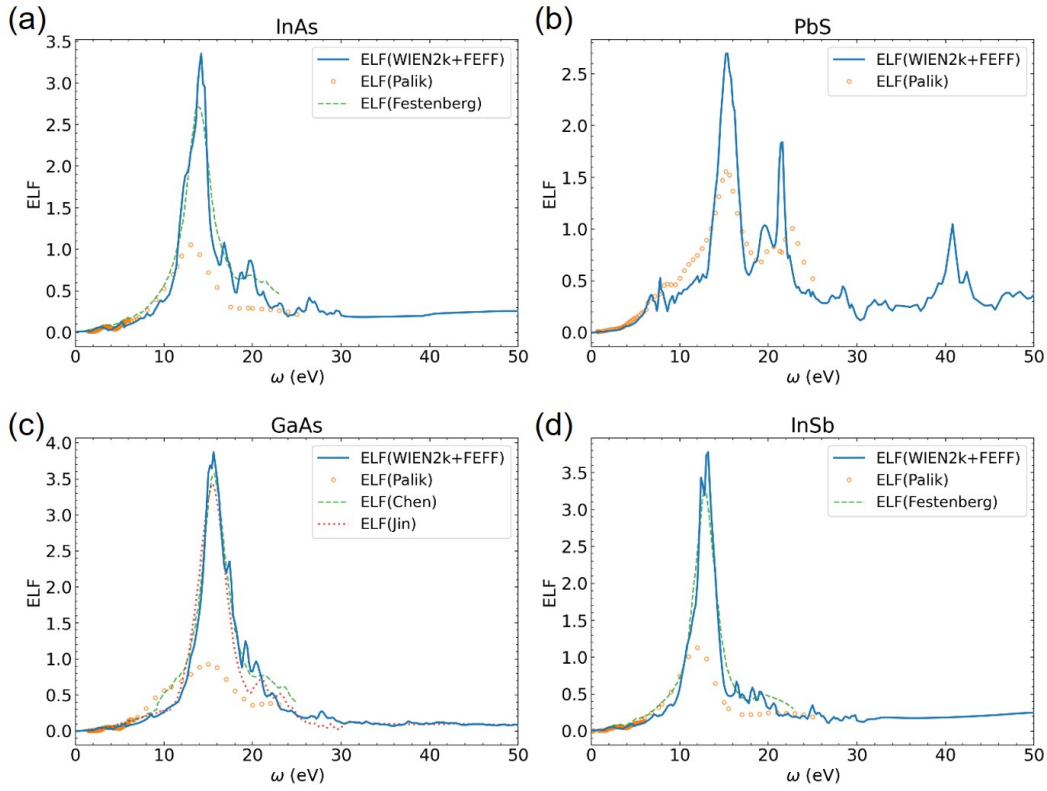

Figure 7: Plots of energy loss functions (ELFs) for (a) InAs, (b) PbS, (c) GaAs, and (d) InSb. Blue solid lines represent ELFs calculated by WIEN2k and FEFF. Orange open circles represent ELFs from the optical data tabulated by Palik [12−14]. Green dashed line represents the ELF measured by Festenberg *et al.* [31] or the ELF as analyzed by Chen *et al.* [32].

GaAs, and InSb were compared with the experimental ELF data. We found that the resulting ELFs are in good agreement with the measured ELFs that obtained from the transmission EELS experiments by von Festenberg [31], analyzed by Chen *et al.* [32], and obtained from measured optical constants by Palik [12−14] and from the reflection EELS experiments by Jin *et al.* [17, 18]. On the other hand, our ELFs are very different from the ELFs that were calculated from experimental optical constants tabulated by Palik. We also compared the band gap energies for 35 materials that were determined from the ELFs calculated by WIEN2k with the measured values. We found that the calculated band gaps for 27 of the 35 materials were smaller than the measured band gaps, and this was consistent with the fact that band gaps obtained through DFT calculations using the local density approximation tend to be smaller than the real band gaps. However, the difference between the calculated and measured band gaps was not so large; the curve fit results of band gaps obtained from WIEN2k, which represents $E_g^{\mathrm{WIEN2k}} = 0.88E_g^{\mathrm{mes}}$ ($\pm 0.06E_g^{\mathrm{mes}}$). The root-mean-square difference for measured and calculated band gaps was 1.0 eV.

We also point out that the resulting 35 ELFs gave excellent sum rule results; the mean absolute percentage error of the *f*-sum and the KK-sum were 1.6% and 0.05%, respectively. Therefore, we can conclude that a sufficiently practical database of the ELFs for compound semiconductors has been constructed.

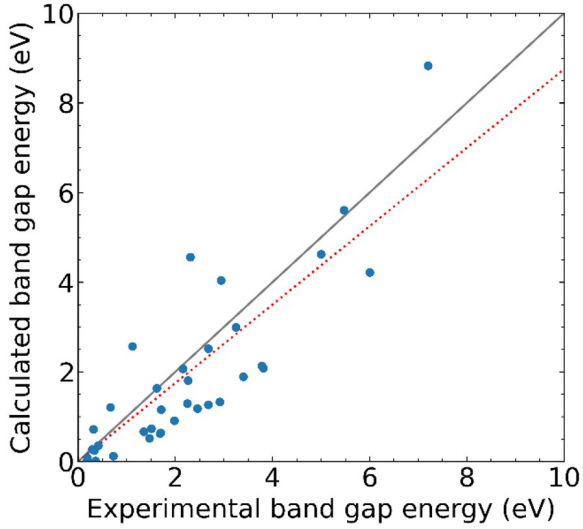

Figure 8: Comparison of calculated band gap energies with experimental values. Solid line represents the case where the measured and calculated band gap values are equal. Dotted line indicates the curve fit result.

Table 3: Number of electrons per molecule Z, Z_{eff} from Eq. (12), $Z_{\mathrm{eff},\varepsilon_2}$ from Eq. (13), P_{eff} from Eq. (14), errors in the *f*-sum rule, and errors in the KK-sum rule for each material.

Material	Z	Z_{eff}	$Z_{\mathrm{eff},\varepsilon_2}$	Error in Z_{eff} (%)	P_{eff}	Error in P_{eff} (%)
AgBr	82	80.1	80.1	–2.29	1.001	0.06
AgCl	64	62.5	62.5	–2.34	1.001	0.06
AgI	100	98.4	98.4	–1.57	1.000	0.01
AlAs	46	46.2	46.2	0.50	1.000	0.00
AlN	20	20.3	20.3	1.26	1.000	–0.02
AlSb	64	62.8	62.8	–1.92	1.000	–0.02
c-BN	12	12.0	12.0	–0.27	1.000	–0.01
h-BN	12	12.2	12.2	1.53	0.999	–0.05
CdS	64	62.9	62.9	–1.78	1.000	0.03
c-CdSe	82	80.4	80.4	–1.99	1.000	0.00
h-CdSe	82	80.4	80.4	–1.99	1.000	0.04
CdTe	100	100.1	100.1	0.10	1.000	0.01
C (diamond)	6	5.9	5.9	–1.13	1.000	0.03
GaAs	64	62.8	62.8	–1.92	1.000	–0.04
GaN	38	37.7	37.7	–0.77	1.000	0.00
GaP	46	45.1	45.1	–2.06	1.000	–0.05
GaSb	82	80.0	80.0	–2.48	0.998	–0.19
GaSe	65	64.0	64.0	–1.54	1.000	–0.04
Ge	32	31.7	31.7	–0.98	1.000	0.04
InAs	82	80.2	80.2	–2.19	0.996	–0.43
InP	64	62.5	62.5	–2.39	1.000	–0.04
InSb	100	97.1	97.1	–2.88	0.997	–0.31
PbS	98	95.4	95.5	–2.64	0.999	–0.09
PbSe	116	112.7	112.8	–2.82	0.999	–0.05
PbTe	134	130.5	130.5	–2.61	1.000	0.00
Se	34	33.9	33.9	–0.40	1.000	0.04
Si	14	13.8	13.8	–1.11	1.000	0.00
c-SiC	20	19.9	19.9	–0.44	1.000	0.04
h-SiC	20	19.9	19.9	–0.29	1.000	0.00
SnTe	102	100.2	100.2	–1.74	0.999	–0.09
Te	52	52.9	52.9	1.74	1.000	–0.03
c-ZnS	46	44.8	44.8	–2.51	1.000	0.00
h-ZnS	46	44.9	44.9	–2.38	1.000	0.00
ZnSe	64	63.2	63.2	–1.33	1.000	–0.01
ZnTe	82	82.3	82.3	0.37	1.000	0.02

Appendix

The Kramers-Kronig relation relates the real and imaginary parts of a complex dielectric function and is expressed as a Cauchy principal-valued integral. Although the integrated function has a singularity, the integral converges if we avoid the singularity properly. Given the discrete data $\{(x_i, y_i)\}_{i=1}^{n}$, we can calculate the Kramers-Kronig integral $S(x_j)$ as follows:

$$S(x_i) = \int_{x_1}^{x_n} \frac{xy(x)}{x^2 - x_j^2}\mathrm{d}x = \sum_{i=1}^{n-1} \int_{x_i}^{x_{i+1}} \frac{xy(x)}{x^2 - x_j^2}\mathrm{d}x. \tag{A1}$$

Here, we assume that $y(x)$ is a polyline connecting each discrete data point:

$$\begin{aligned} y(x) &= b_i + c_i x \ (x_i < x < x_{i+1}), \\ c_i &= \frac{y_{i+1} - y_i}{x_{i+1} - x_i}, \quad b_i = y_i - c_i x_i, \qquad \text{for } i = 1, 2, \ldots, n-1 \end{aligned} \tag{A2}$$

$\{x_i\}_{i=1}^{n}$ need not be equally spaced. When the integral range is independent of the singularity, $x = x_j$, i.e., $x_1 \le x \le x_{j-1}$ or $x_{j+1} \le x \le x_n$, the integral of each interval can be calculated as follows:

$$\int_{x_i}^{x_{i+1}} \frac{x(b_i + c_i x)}{x^2 - x_j^2} \mathrm{d}x = \frac{1}{2}\int_{x_i}^{x_{i+1}} \left(\frac{b_i + c_i x}{x - x_j} + \frac{b_i + c_i x}{x + x_j} \right) \mathrm{d}x$$
$$= c_i(x_{i+1} - x_i) + \frac{1}{2}\left[(b_i + c_i x_j) \log \left| \frac{x_{i+1} - x_j}{x_i - x_j} \right| + (b_i - c_i x_j) \log \left| \frac{x_{i+1} + x_j}{x_i + x_j} \right| \right]. \quad \text{(A3)}$$

For the remaining integration range $x_{j-1} \le x \le x_{j+1}$ sandwiching the singularity $x = x_j$, two intervals are integrated together to prevent divergence of the integrals:

$$s = P. \int_{x_{j-1}}^{x_{j+1}} \frac{xy(x)}{x^2 - x_j^2} \mathrm{d}x, \quad \text{(A4)}$$

where symbol P represents Cauchy's principal value. We evaluated the integral by performing Cauchy's principal-valued integral. The replacement $(x_{j-1}, x_j, x_{j+1}, y_{j-1}, y_j, y_{j+1}, b_{j-1}, c_{j-1}, b_j, c_j) \to (x_1, x_2, x_3, y_1, y_2, y_3, b_1, c_1, b_2, c_2)$ was then made to simplify the equation as follows:

$$s = P. \int_{x_1}^{x_3} \frac{xy(x)}{x^2 - x_2^2} \mathrm{d}x = \lim_{\varepsilon \to +0} \left[\int_{x_1}^{x_2 - \varepsilon} \frac{x(b_1 + c_1 x)}{x^2 - x_2^2} \mathrm{d}x + \int_{x_2 + \varepsilon}^{x_3} \frac{x(b_2 + c_2 x)}{x^2 - x_2^2} \mathrm{d}x \right]$$
$$= c_1(x_2 - x_1) + c_2(x_3 - x_2) + \frac{b_1 - c_1 x_2}{2} \log \left| \frac{2x_2}{x_1 + x_2} \right| + \frac{b_2 - c_2 x_2}{2} \log \left| \frac{x_3 + x_2}{2x_2} \right| \quad \text{(A5)}$$
$$+ \frac{b_1 + c_1 x_2}{2} \log \left| \frac{1}{x_1 - x_2} \right| + \frac{b_2 + c_2 x_2}{2} \log |x_3 - x_2| + \left(\frac{b_1 + c_1 x_2}{2} - \frac{b_2 + c_2 x_2}{2} \right) \lim_{\varepsilon \to +0} \{\log |\varepsilon|\}.$$

Noticing that $b_1 + c_1 x_2 = b_2 + c_2 x_2 = y_2$, we find that the last term vanishes. Further simplification of some of the terms gives:

$$s = (y_3 - y_1) - \frac{b_1 - c_1 x_2}{2} \log \left| \frac{1}{2}\left(1 + \frac{x_1}{x_2}\right) \right| + \frac{b_2 - c_2 x_2}{2} \log \left| \frac{1}{2}\left(1 + \frac{x_3}{x_2}\right) \right| + \frac{y_2}{2} \log \left| \frac{x_3 - x_2}{x_1 - x_2} \right|. \quad \text{(A6)}$$

Finally, $S(x_j)$ is calculated from the sum of the results of all integration ranges. Note that regression of the three points around singular point $x = x_j$ using a quadratic function is inappropriate because it will cause overfitting.

References

[1] U. Fano, Phys. Rev. **103**, 1202 (1956).
[2] C. J. Powell and A. Jablonski, J. Phys. Chem. Ref. Data **28**, 19 (1999).
[3] S. Tanuma, C. J. Powell, and D. R. Penn, Surf. Interface Anal. 11, **577** (1988).
[4] S. Tanuma, C. J. Powell, and D. R. Penn, Surf. Interface Anal. 17, **911** (1991).
[5] S. Tanuma, C. J. Powell, and D. R. Penn, Surf. Interface Anal. 17, **927** (1991).
[6] S. Tanuma, C. J. Powell, and D. R. Penn, Surf. Interface Anal. 21, **165** (1994).
[7] S. Tanuma, C. J. Powell, and D. R. Penn, Surf. Interface Anal. 43, **689** (2011).
[8] H. Shinotsuka, S. Tanuma, C. J. Powell, and D. R. Penn, Surf. Interface Anal. **47**, 871 (2015).
[9] H. Shinotsuka, S. Tanuma, C. J. Powell, and D. R. Penn, Surf. Interface Anal. **47**, 1132 (2015).
[10] H. Shinotsuka, B. Da, S. Tanuma, H. Yoshikawa, C. J. Powell, and D. R. Penn, Surf. Interface Anal. **49**, 238 (2016).
[11] H. Shinotsuka, S. Tanuma, C. J. Powell, and D. R. Penn, Surf. Interface Anal. **51**, 427 (2018).
[12] E. D. Palik (Ed.), *Handbook of Optical Constants of Solids*, Vol. 1 (Academic Press, New York, 1985).
[13] E. D. Palik (Ed.), *Handbook of Optical Constants of Solids*, Vol. 2 (Academic Press, New York, 1991).
[14] E. D. Palik (Ed.), *Handbook of Optical Constants of Solids*, Vol. 3 (Academic Press, New York, 1998).
[15] S. E. Schnatterly, in: *Solid State Physics*, Vol. 34, edited by H. Ehrenreich, F. Seitz, and D. Turnbull (Academic Press, New York, 1979) p. 275.
[16] C. J. Powell, in: *Electron Beam Interactions with Solids for Microscopy, Microanalysis, and Microlithography*, edited by D. F. Kyser, D. E. Newbury, H. Niedrig, and R. Shimizu (Scanning Electron Microscopy, Chicago, 1984) p. 19.
[17] H. Jin, H. Shinotsuka, H. Yoshikawa, H. Iwai, S. Tanuma, and S. Tougaard, J. Appl. Phys. **107**, 083709 (2010).
[18] H. Jin, H. Shinotsuka, H. Yoshikawa, H. Iwai, M. Arai, S. Tanuma, and S. Tougaard, Surf. Interface Anal. **45**, 985 (2013).
[19] A. L. Ankudinov, C. E. Bouldin, J. J. Rehr, J. Sims, and H. Hung, Phys. Rev. B **65**, 104107 (2002).
[20] P. Blaha, K. Schwarz, G. K. H. Madsen, D. Kvasnicka, and J. Luitz, *WIEN2k, An Augmented Plane Wave Plus Local Orbitals Program for Calculating Crystal Properties* (Vienna University of Technology, Vienna, 2001).
[21] J. P. Perdew, K. Burke, and M. Ernzerhof, Phys. Rev. Lett. **77**, 3865 (1996).
[22] W. S. M. Werner, K. Glantschnig, and C. Ambrosch-Draxl, J. Phys. Chem. Ref. Data **38**, 1013 (2009).
[23] B. L. Henke, P. Lee, T. J. Tanaka, R. L. Shimabukuro, and B. K. Fujikawa, in: *Low Energy X-ray Diagnostics*, edited by D. T. Attwood and B. L. Henke (American Institute of Physics, New York, 1981) p. 340.
[24] J. J. Rehr, M. P. Prange, and J. J. Kas, J. Phys.: Conf. Ser. **190**, 012001 (2009).
[25] M. P. Prange, J. J. Rehr, G. Rivas, J. J. Kas, and J. W. Lawson, Phys. Rev. B **80**, 155110 (2009).

[26] A. P. Sorini, J. J. Kas, J. J. Rehr, M. P. Prange, and Z. H. Levine, Phys. Rev. B **74**, 165111 (2006).
[27] G. D. Mahan, *Many-Particle Physics*, 3rd ed. (Kluwer Academic/Plenum Publishers, New York, 2000).
[28] AtomWork database (https://crystdb.nims.go.jp/en/).
[29] Materials data repository provided by the National Institute for Materials Science (https://mdr.nims.go.jp/).
[30] S. Tanuma, C. J. Powell, and D. R. Penn, Surf. Interface Anal. **20**, 77 (1993).
[31] C. v. Festenberg, Z. Phys. A **227**, 453 (1969).
[32] Y. F. Chen, C. M. Kwei, and C. J. Tung, Phys. Rev. B **48**, 4373 (1993).
[33] H. R. Philipp and H. Ehrenreich, Phys. Rev. **129**, 1550 (1963).
[34] J. P. Perdew and A. Zunger, Phys. Rev. B **23**, 5048 (1981).

Published by The Japan Society of Vacuum and Surface Science